Accepted Manuscript

Kindlin-1 regulates epidermal growth factor receptor signalling

Magdalene Michael, Rumena Begum, Grace K. Chan, Austin J. Whitewood, Daniel R. Matthews, Benjamin T. Goult, John A. McGrath, Maddy Parsons

PII: S0022-202X(18)32587-9

DOI: 10.1016/j.jid.2018.08.020

Reference: JID 1584

To appear in: *The Journal of Investigative Dermatology*

Received Date: 7 May 2018

Revised Date: 9 August 2018

Accepted Date: 10 August 2018

Please cite this article as: Michael M, Begum R, Chan GK, Whitewood AJ, Matthews DR, Goult BT, McGrath JA, Parsons M, Kindlin-1 regulates epidermal growth factor receptor signalling, *The Journal of Investigative Dermatology* (2018), doi: https://doi.org/10.1016/j.jid.2018.08.020.

Kindlin-1 regulates epidermal growth factor receptor signalling

Magdalene Michael[1], Rumena Begum[1,2], Grace K. Chan[1], Austin J. Whitewood[3], Daniel R Matthews[4], Benjamin T. Goult[3], John A. McGrath[1], Maddy Parsons[2,4,5]

[1] Randall Division of Cell and Molecular Biophysics, King's College London, Guy's Campus, London, SE1 1UL, UK.

[2] St Johns Institute of Dermatology, King's College London, Guys Campus, London, SE1 9RT, UK.

[3] School of Biosciences, University of Kent, Canterbury, Kent, CT2 7NJ, UK

[4] Nikon Imaging Centre, King's College London, Guy's Campus, London SE1 1UL, UK

[5] To whom correspondence should be addressed: maddy.parsons@kcl.ac.uk

Running title: Kindlin-1 stabilises EGFR

ABSTRACT

Kindler syndrome (KS) is an autosomal recessive genodermatosis that results from mutations in the *FERMT1* gene encoding t kindlin-1. Kindlin-1 localises to focal adhesion and is known to contribute to the activation of integrin receptors. Most cases of KS show a reduction or complete absence of kindlin-1 in keratinocytes, resulting in defective integrin activation, cell adhesion and migration. However, roles for kindlin-1 beyond integrin activation remain poorly defined. In the current study we show that skin and keratinocytes from KS patients have significantly reduced expression levels of the epidermal growth factor receptor (EGFR), resulting in defective EGF-dependent signalling and cell migration. Mechanistically, we demonstrate that kindlin-1 can associate directly with EGFR in vitro and in keratinocytes in an EGF-dependent, integrin-independent manner and that formation of this complex is required for EGF-dependent migration. We further demonstrate that kindlin-1 acts to protect EGFR from lysosomal-mediated degradation. This reveals a new role for kindlin-1 that has implications for understanding KS disease pathology.

KEYWORDS:

kindlin-1/EGFR/keratinocyte/migration/adhesion

INTRODUCTION

Kindler syndrome (KS; OMIM 173650) is a rare autosomal recessive skin disorder, for which there is currently no cure. Genome-wide linkage analysis showed that KS is caused by an abnormality in the actin cytoskeleton and its association with the extracellular matrix (ECM) due to a deficiency or defect in the focal adhesion protein, kindlin-1 (also known as fermitin family homologue 1) (Jobard et al., 2003, Siegel et al., 2003)). Clinical features of KS range from trauma-induced blistering, progressive poikiloderma and skin atrophy, photosensitivity, destructive periodontal disease, severe colitis and squamous cell carcinoma (Ashton, 2004, Lai-Cheong et al., 2007). Since identifying the *FERMT1* gene, at least 170 patients and 60 mutations have been reported. These mutations include nonsense, frameshift splice site and internal deletion changes all resulting in loss of expression (Has et al., 2011, Techanukul et al., 2011). The human *FERMT1* gene encodes the protein kindlin-1 and other members of this protein family include kindlin-2 and kindlin-3 (Siegel et al., 2003). Although related, these proteins exhibit differential expression patterns: Kindlin-1 expression is predominantly restricted to epithelial cells, kindlin-2 is widely expressed and kindlin-3 is present in haematopoietic and endothelial cells (Bialkowska et al., 2010, Lai-Cheong et al., 2009, Siegel et al., 2003, Wiebe et al., 2008). Both kindlin-1 and kindlin-2 localise to focal adhesions and kindlin-2 is also recruited to cell-cell junctions (Brahme et al., 2013, Lai-Cheong et al., 2008), while kindlin-3 localises to podosomes (Meves et al., 2009). All kindlins have a bipartite FERM (4.1 protein, ezrin, radixin, moesin) domain, consisting of four subdomains (F0, F1, F2 and F3) that are present in many proteins involved in cytoskeletal organisation (Baines et al., 2014, Goult et al., 2009). The kindlin F2 subdomain differs to other FERM domain proteins through an insertion of a pleckstrin homology (PH) domain, that binds phosphoinositide phosphates (Meves et al., 2009).

Kindlins have all been shown to bind directly to the cytoplasmic domain of β-integrin subunits and contribute to integrin activation (Rognoni et al., 2016). In normal skin, kindlin-1 localises in basal keratinocytes at the dermal-epidermal junction and accumulates at cell-matrix adhesion sites. In isolated keratinocytes, kindlin-1 localises to the cell leading edge and focal adhesions (Larjava et al., 2008). Depletion of kindlin-1 leads to reduced proliferation, adhesion and spreading as well as reduced directed migration, with the cells displaying multiple leading edges and multipolar shapes (Has et al., 2008, Herz et al., 2006, Zhang et al., 2016). The role of kindlin-1 in integrin-mediated processes provides explanation for some of the clinical features observed in patients with KS. Potential non-integrin related roles for kindlin-1 in controlling cell behaviour remain unclear.

In this study we performed mass spectrometry analysis of keratinocytes from KS patients and identified significantly reduced levels of the epidermal growth factor receptor (EGFR) in KS samples. Further analysis demonstrated defective downstream signalling of EGFR and attenuated cell responses to EGF stimulation. The expression of kindlin-1 in KS cells was able to restore EGFR expression levels and responses to EGF. Our investigations revealed a direct interaction between kindlin-1 and EGFR at the plasma membrane that acts to protect EGFR from lysosomal degradation, independently of kindlin-1 binding to integrins. This data provides new insight into kindlin-1 function in keratinocytes and may provide new avenues for pursuit of therapeutic strategies to treat KS patients.

RESULTS AND DISCUSSION

KS keratinocytes have reduced levels of EGFR and attenuated response to EGF stimulation

In order to identify new pathways downstream of kindlin-1, we profiled lysates of keratinocytes from healthy donors (WT) and two different KS patients using mass spectrometry. This analysis revealed a reduction in protein levels of EGFR in KS keratinocytes, which was verified using western blotting (Figure 1A). However, no change in mRNA levels of EGFR was detected in KS cells by semi-quantitative RT-PCR (Figure 1B). Analysis of normal human lung (16HBE) and breast (MCF10A) epithelial cell lines also revealed a reduction of EGFR levels upon siRNA depletion of kindlin-1 (Supplementary Figures 1A, 1B), suggesting a common role for kindlin-1 in regulating EGFR levels in human epithelial cells. Exogenous expression of kindlin-1 in keratinocytes restored EGFR levels (Figure 1C) thereby specifically attributing this phenotype to kindlin-1 expression. Taken together these findings demonstrate a global reduction in EGFR levels when kindlin-1 is absent or depleted. Further analysis by FACs analysis confirmed a reduction in EGFR surface levels in KS keratinocytes (Figure 1D). Moreover, immunostaining of healthy donor and KS patient skin sections showed a striking reduction of EGFR in the basal keratinocytes in KS skin compared to WT (Figure 1E).

EGFR regulates a number of signalling pathways, that act to regulate keratinocyte survival, growth, adhesion and migration (Bakker et al., 2017). To examine the effect of loss of kindlin-1 on EGFR signalling, cells were starved overnight, stimulated with EGF for 10 minutes and the phosphorylation of EGFR (Figure 1F) and its downstream effector ERK1/2 (Figure 1G) assessed. As expected, EGFR phosphorylation in response to EGF was significantly reduced in KS keratinocytes, in-line with the constitutively lower levels of EGFR in these cells (Figure 1F), with a resulting loss of EGF-dependent ERK1/2 phosphorylation (Figure 1G). To determine whether this loss of EGF responsiveness had an impact on functional cell behaviour, we assessed migratory responses to EGF by time-lapse

microscopy. Data demonstrated that KS cells exhibited higher migration speeds compared to WT cells under starved conditions, as we have shown previously (Supplementary Figures 1C,D; (Maiuri et al., 2012)). Addition of EGF led to increased WT keratinocytes migration rates but had no effect on KS cell speed, confirming a failure to respond to EGF in the absence of kindlin-1. Migration speeds were rescued in KS cells re-expressing mCherry-kindlin-1, confirming that the observed phenotypes were due to loss of kindlin-1 expression (Supplementary Figures 1D,E). Together these findings demonstrate that kindlin-1 deficient human keratinocytes have reduced EGFR levels resulting in impaired responses to EGF.

Kindlin-1 regulates subcellular distribution and dynamics of EGFR

To determine whether the reduced levels of EGFR in KS cells coincided with altered subcellular distribution, we analysed the localisation of EGFR in sparsely plated WT and KS keratinocytes following EGF stimulation. Total and surface levels of EGFR were quantified by measuring the mean fluorescence intensities of either the whole cell area or plasma membrane. Consistent with the western blot analyses (Figure 1A,F), EGF stimulation did not alter the relative intensity of EGFR in either cell type but there was a marked reduction in total EGFR levels in KS cells (Figures 2A-C). In starved WT cells, EGFR was localised at the plasma membrane and cytoplasmic compartments, whilst KS cells showed very weak EGFR staining at the plasma membrane with increased accumulation in perinuclear compartments (Figures 2A-C). Following EGF treatment, EGFR redistributed from the plasma membrane into perinuclear compartments in WT cells, coincident with reduced EGFR at the plasma membrane (Figure 2C). In contrast, EGFR remained in the perinuclear compartments of KS cells following EGF stimulation (Figure 2C). Kindlin-2 has been shown previously to be expressed at normal levels in KS patients (Lai-Cheong et al., 2008) suggesting it is not disrupted upon loss of kindlin-1, but also cannot functionally replace

kindlin-1 in these cells. However, in order to determine whether loss of kindlin-1 and resulting EGFR mislocalisation could be compensated for overexpression of kindlin-2, WT and KS cells were transfected with GFP-kindlin-2 and total and surface EGFR levels analysed by confocal microscopy. Data demonstrated that kindlin-2 overexpression had no effect on EGFR levels or localisation in either WT or KS keratinocytes (Supplementary Figures 1E,F) suggesting kindlin-2 cannot compensate for loss of kindlin-1 in these cells. Indeed, functional non-redundant roles for kindlins-1 and-2 have also been suggested in the context of integrin binding in keratinocytes (Bandyopadhyay et al., 2012), further supporting the notion that these proteins have different roles in epithelial cell function.

EGFR is known to undergo endocytosis and, depending on the cell type and EGF concentration, can be recycled back to the plasma membrane or routed for degradation (Bakker et al., 2017). To determine whether kindlin-1 may play a role in regulating EGFR dynamics at the plasma membrane, we analysed WT and KS cells stably expressing EGFR-GFP following fluorescence recovery after photobleaching (FRAP) at the plasma membrane under growth conditions. Despite expressing lower levels of EGFR, KS cells showed enhanced early recovery profiles compared to WT and reduced T1/2 speed, without changing the mobile fraction (Supplementary Figure 2A). We confirmed this effect of kindlin-1 was not due to global changes in clathrin-mediated endocytosis, as transferrin-Texas Red uptake assays revealed no differences between WT and KS cells (Supplementary Figure 2B), indicating that global receptor internalisation was unperturbed by the loss of kindlin-1. Notably, inhibition of dynamin activity, but not recycling (through dynasore and primaquine treatment respectively) resulted in a slower fluorescence recovery T1/2 and reduced EGFR mobile fraction (Supplementary Figures 2C,D). This data demonstrates that loss of kindlin-1

destabilises EGFR under steady state conditions and that inhibition of EGFR internalisation, but not receptor recycling, reduces EGFR dynamics at the plasma membrane.

To determine potential kindlin-1-dependent changes in EGFR subcellular compartmentalisation, we used colocalisation analysis to study EGFR localisation with key endocytic markers at time points following EGFR stimulation: early endosomes (EEA1, 10min), lysosomes (LAMP1, 30min) and recycling endosomes (Rab11a, 1hr). Pearson's correlation analysis revealed significantly reduced colocalisation between EGFR/EEA1 and EGFR/Rab11 in KS cells compared to WT (Figure 2D and 2F). In contrast, a significant increase in colocalisation between EGFR and LAMP1 was observed in KS cells compared to WT (Figure 2E). To further explore the real-time dynamics of the EGFR positive compartments following EGF stimulation, we performed live cell imaging on WT and KS cells expressing EGFR-GFP, cherry-Rab11a and labelled with lysotracker far red, for 30min post-EGF stimulation. Upon addition of EGF, EGFR positive vesicles moved in a retrograde fashion from the plasma membrane into the cell interior, increasing in number and size over time (Figure 2G,H; Movie 1). In contrast, EGFR labelled vesicles in KS cells displayed random movement in the perinuclear region throughout the 30min observed with the size and vesicle number remaining largely unaltered (Figure 2G,H; Movie 2). Analysis of overlapping pixels in the EGFR-GFP and lysotracker labelled vesicles confirmed the LAMP1 data in fixed cells (Figure 2E), showing a constitutively higher colocalisation between EGFR positive vesicles and lysosomal compartments in KS cells compared to WT cells throughout the period of EGF stimulation (Figure 2I).

Kindlin-1 regulates cellular EGFR levels by restricting lysosomal degradation of EGFR

EGFR is subject to ligand-induced degradation via the lysosomal or proteasomal pathways (Singh and Coffey, 2014). Given the increased EGFR within lysosomal compartments in KS cells, we next analysed whether EGFR was reduced in KS cells due to enhanced protein degradation. Treatment of WT and KS cells with the proteasome inhibitor MG132 did not change EGFR levels in KS cells (Figure 3A,D). However, treatment with lysosomal inhibitors leupeptin or concanamycin A (ConA) restored EGFR expression in KS cells up to WT levels (Figure 3B-D) suggesting loss of kindlin-1 leads to increased lysosomal-dependent EGFR degradation. EGFR binds to the E3 ubiquitin ligase c-Cbl in response to EGF, either at the plasma membrane or on early endosomes, which in turn promotes poly-ubiquitination of EGFR resulting in degradation (Duan et al., 2003). To determine whether kindlin-1-dependent changes to EGFR altered c-Cbl association with the receptor, we analysed c-Cbl-EGFR binding by co-IP in WT and KS cells treated with DMSO or ConA under growth conditions. A dramatic increase in c-Cbl binding to EGFR in KS cell lysates was observed, with or without treatment with ConA (Figure 3E), suggesting that increased constitutive c-Cbl binding in the absence of kindlin-1 may result in increased targeting of EGFR for lysosomal degradation.

Kindlin-1 directly interacts with EGFR

Kindlin-2 has previously been suggested to directly interact with EGFR through an association with the EGFR kinase domain (Guo et al., 2015). In order to determine whether kindlin-1 could interact with EGFR, Individual domains of kindlin-1 were generated as GST fusion proteins and used to pull out endogenous EGFR from cell lysates (Figure 4A). Full length GST-kindlin-1 (GST1) bound to EGFR and a consistently strong binding with the F1 domain of kindlin-1 was also observed (GST3; Figure 4B). The F1 domain contains an unstructured loop that we postulated could be a potential binding region for EGFR

(Bouaouina et al., 2012). We tested this hypothesis by expressing a His-tagged F1loop to capture EGFR from cell lysates. As predicted, the F1loop bound strongly to EGFR in cell lysates in contrast to the His-kinesin light chain domain that served as a negative control (Figure 4C). To test whether association between kindlin-1 and EGFR was direct, a GST fusion of the EGFR cytoplasmic domain was incubated with His-F1loop of kindlin-1 in solution. Pulldown of the GST-EGFR cytoplasmic tail revealed a strong interaction with the His-kindlin-1 F1 loop (Figure 4D), indicating a direct interaction between the two proteins. Moreover, assessment of binding kinetics between these proteins by microscale thermophoresis (MST) revealed a robust interaction between the EGFR cytoplasmic tail membrane proximal region and both full length and F0F1 domains of kindlin-1 (Figure 4E). Taken together this data demonstrates that kindlin-1 binds directly to the EGFR cytoplasmic domain via the kindlin-1 F1 loop. Moreover, as c-Cbl binding is significantly and constitutively enhanced in cells lacking kindlin-1 (Figure 3E), this would suggest that binding of kindlin-1 to the EGFR cytoplasmic tail restricts binding of c-Cbl, leading to retention of EGFR at the plasma membrane, enhanced signalling and reduced degradation.

To further define when and where kindlin-1 may associate with EGFR in cells, we analysed their relative subcellular distributions using live-cell structure illumination microscopy (SIM) super-resolution imaging of KS cells expressing mCherry-kindlin-1 and EGFR-GFP. Images and subsequent analysis showed that colocalisation between the two proteins occurred within the first 15mins of EGF stimulation at the plasma membrane (Figure 5A, Supplementary Figure 3A). We were also unable to detect any kindlin-1 co-localising with EGFR within endosomes. Immunoprecipitation of endogenous EGFR from KS cells re-expressing mCherry-kindlin1 also revealed that kindlin1 forms a complex with EGFR in a time-dependent manner, with strongest interactions occurring 5 minutes following EGF

stimulation and resuming to basal levels by 60 minutes (Figure 5B). However, we were unable to detect kindlin-2 in these immunoprecipitated complexes (Supplementary Figure 3B), suggesting the binding of kindlin-1 may be specific in keratinocytes.

Analysis of direct binding between the two proteins using fluorescence lifetime imaging microscopy (FLIM) to analyse fluorescence resonance energy transfer (FRET) also revealed a direct interaction between EGFR-GFP and mCherry-kindlin-1 in cells that was increased following 10 minutes of EGF stimulation (Figure 5C). Moreover, kindlin-1:EGFR binding was independent of kindlin-1:integrin binding as FRET-FLIM analysis demonstrated strong, constitutive interaction between EGFR-GFP and mCherry-W612Akindlin-1, which is defective in integrin binding (Supplementary Figure 3C; (Bouaouina et al., 2012, Huet-Calderwood et al., 2014)). Further analysis of these cells demonstrated that expression of mCherry-W612Akindlin-1 in KS cells was also able to partially restore the migration response to EGF (Supplementary Figure 3D), further indicating that kindlin-1:EGFR binding plays an important role in control of EGF responses and that this can act at least in part independently of kindlin-1:integrin complex formation.

To explore whether EGFR kinase activity regulates kindlin-1-EGFR binding, we assessed the colocalisation between endogenous EGFR and GFP-kindlin-1 expressed in KS cells in the presence of either DMSO or AG1478, an EGFR-specific tyrosine kinase inhibitor. Inhibition of EGFR activity resulted in an increase in colocalisation between EGFR and GFP-kindlin-1 (Figure 5D), potentially through enrichment of EGFR at the plasma membrane. Finally, as kindlin-2 has previously been suggested to be tyrosine phosphorylated (Liu et al., 2015, Qu et al., 2014), we sought to determine whether the same modification on kindlin-1 could occur through EGFR-mediated signalling. IP analysis demonstrated that GFP-kindlin-1 was

tyrosine phosphorylated under basal conditions (Figure 5E). However, treatment with AG1478 had no effect on kindlin-1 tyrosine phosphorylation levels, suggesting kindlin-1 is constitutively tyrosine phosphorylated in growth conditions and this does not depend on signals downstream of active EGFR.

In summary, our data demonstrates a direct interaction between kindlin-1 and EGFR that acts to restrict c-Cbl-EGFR association and thus protect EGFR from lysosomal degradation. Whilst our data does not allow us to conclusively state that EGFR-Cbl binding in KS cells is constitutive, our data does support the notion that the presence of kindlin-1 is required to ensure correct regulation of the EGFR-Cbl complex. Our proposed model is that binding of kindlin-1 to the EGFR cytoplasmic tail can displace Cbl binding and potentially act to stabilise EGFR at the membrane, and subsequently control modulation of EGFR routing to the endo-lysosomal system. Loss of kindlin-1 expression in patients with KS results in lower EGFR levels in the skin and isolated keratinocytes, resulting in loss of EGF-induced signalling and migratory behaviour. This newly described function for kindlin-1 is very likely to contribute to the clinical features observed in KS patients in agreement with our recent discovery of an EGFR loss of function mutation in patients with skin fragility (Campbell et al., 2014). Based on our data, investigations of strategies to modulate EGFR stability may represent a valid therapeutic avenue for treating skin fragility patients in future.

MATERIALS AND METHODS

Plasmids and siRNAs

GFP-kindlin-1, GFP-kindlin-1W612A and GFP-kindlin-2 constructs were generously provided by Prof David Calderwood (Yale University, USA; (Bouaouina et al., 2012, Huet-

Calderwood et al., 2014)). EGFR-GFP was provided by Dr Andy Reynolds (AstraZeneca UK; (Reynolds et al., 2003)). EGFR cytoplasmic domain GST fusion constructs were generously provided by Bob Adelstein (NIH; (Kim et al., 2012)). Murine full length kindlin-1 and kindlin-1 F0F1 (1-275) were cloned into a pET151 vector (Invitrogen). Cherry-kindlin1 and cherry-kindlin1W612A lentiviral constructs have been previously described (Zhang et al., 2016). mCherry-Rab11a was a gift from Dr Patrick Caswell (University of Manchester, UK; (Caswell et al., 2007)).

RT-PCR

RNA extraction from cells was performed using RNAeasy Mini Kit (Qiagen) and reverse transcription of RNA was carried out using RevertAid Reverse Transcriptase (Thermo Scientific), according to manufacturer's instructions. RT-PCR primer sequences are as follows: GAPDH (forward 5'-AGAAGGCTGGGGCTCATTTG-3', reverse 5'-AGGGGCCATCCACAGTCTTC-3'); kindlin-1 (forward 5'-TCAAACAGTGGAATGTAAACTGG-3', reverse 5'-TACATGCTGGGCACGTTAGG-3').

Cell culture and transfections

Immortalised WT keratinocytes and those from a KS patient (harbouring the mutation c.676insC/c.676insC) have both been previously described (Lai-Cheong et al., 2007, Zhang et al., 2016). The original study in which the cells were isolated was conducted according to the principles of the Declaration of Helsinki. All cells were obtained under the St. Thomas Hospital Ethics Committee-approved project "Molecular basis of inherited skin disease—07/H0802/104" and following written consent by the participating individuals. Both cell lines were grown in serum-free keratinocyte growth medium (SFM) containing EGF and bovine pituitary extract (Gibco) and supplemented with penicillin and streptomycin. HEK293T cells

were cultured in Dulbecco's modified Eagle's medium (DMEM) supplemented with penicillin and streptomycin, L-glutamine and 10% fetal bovine serum (FBS). 16HBE cells were grown in Minimum Essential Media (MEM) supplemented with penicillin and streptomycin, L-glutamine and 10% FBS. MCF10A cells were cultured in DMEM supplemented with penicillin and streptomycin, L-glutamine, 5% horse serum, EGF (20 ng/mL), hydrocortisone (0.5 μg/mL), cholera toxin (100 ng/mL) and insulin (10 μg/mL). HEK 293T transfections were performed using PEI transfection reagent at a 1:7 ratio of DNA: PEI reagent. Keratinocyte transfection of plasmids was carried out using Attractene transfection reagent (Qiagen) and all siRNA transfections were performed using Dharmofect transfection reagent (Dharmacon), in accordance to manufacturer's instructions. Inhibitors were all purchased from Sigma and used at the following concentrations: Leupeptin (100 nM, 4 hours), MG132 (20 μM, 4 hours), Concanamycin A (100 nM, 16 hours), dynasore (80 μM, 1 hour), primaquine (100 μM, 1 hour) and AG1478 (5 nM, 1 hour).

Antibodies

Primary antibodies used: EGFR (for WB; Cell Signaling), EGFR (for IP; Cell Signaling), EGFR (for IF; Santa Cruz); kindlin-2 (Abcam); phospho-EGFR Y1173 (Cell Signaling), phospho-tyrosine (4G10; Millipore), GFP (Roche), HA (Cell Signaling), c-Cbl (Cell Signaling), GAPDH (Genetex), HSC70 (Santa Cruz), EEA1 (Cell Signaling), LAMP1 (Cell Signaling), phospho-ERK1/2 (Cell Signaling), ERK1/2 (Cell Signaling), GST (Sigma), His (HRP conjugate; Millipore). All anti-species HRP conjugated secondary antibodies were from Dako and all AlexaFluor conjugated antibodies from Molecular Probes. Other reagents and suppliers were: Phalloidin AlexaFluor (Molecular Probes), Hoechst (Sigma), lysotracker deep red (Molecular Probes), transferrin Texas Red (ThermoFisher Scientific).

GST and His tag protein purification

Protein production was induced in E.coli BL21 bacterial strains with IPTG (100 μM) overnight at 18°C. For GST-tagged proteins, bacterial pellets were re-suspended in 50 mM Tris, 300 mM NaCl, pH 8.0 in the presence of protease inhibitors, sonicated and cleared by centrifugation. The protein solution was then incubated with glutathione sepharose beads (GE Healthcare) for 2 hours at 40°C followed by three washes in 50 mM Tris, 300mM NaCl, pH 8.0 with 2 mM β-mercaptoethanol. The GST-tagged proteins were either left bound to the beads (for GST pulldown experiments) or eluted with glutathione solution (50 mM Tris, 300 mM NaCl, 40 mM glutathione, pH 8.0) and dialysed overnight. For His-tagged proteins, bacterial pellets were re-suspended in His lysis buffer (25 mM HEPES pH 8.0, 500 mM NaCl, 10 mM imidazole) containing protease inhibitors, sonicated and cleared by centrifugation. Nickel NTA beads (Qiagen) were incubated with the protein solution for 2 hours at 4°C followed by three washes in lysis buffer containing 50 mM imidazole. The His-tagged proteins were eluted from the beads with lysis buffer containing 250 mM imidazole, followed by overnight dialysis. For MST analysis, standard nickel-affinity chromatography was used to purify the His-tagged recombinant proteins as described previously (Banno et al., 2012). Purified samples were analysed by SDS-PAGE on a 10% gel and stained using Coomassie blue. Protein concentrations were determined using the respective extinction coefficients at 280 nm calculated using ProtParam.

GFP traps, immunoprecipitation (IP) and western blotting

Cells were lysed in cold lysis buffer (50 mM Tris-HCL pH 7.4, 200 mM NaCl, 1% NP-40, 2 mM MgCl2, 10% glycerol) containing protease inhibitors and phosphatase inhibitors and lysates were cleared by centrifugation. For GFP traps, the cleared lysates were incubated with

GFP trap beads for 2 hours at 4^0C, followed by three washes in lysis buffer. For other IPs, cleared lysates were incubated with either antibody or species matched IgG overnight and then incubated for 2 hours with Protein A/G beads (pre-blocked with 0.2% BSA). Beads were washed three times in lysis buffer and resuspended in sample buffer, boiled for 10 min and resolved on a 12% SDS-PAGE gel. For mass spectrometry analysis, WT and KS lysates were resolved on 10% SDS PAGE gels, silver stained and identified bands were excised and sent for processing and analysis to Aberdeen Proteomics (University of Aberdeen, School Medical Sciences, Aberdeen).

Flow cytometry

FACS analysis was performed as previously described (Worth et al., 2010). Briefly, cells were scraped with PBS and fixed with 4% PFA for 20 min. Cells were then blocked in PBS containing 2% BSA, incubated with primary antibody with 90 min, washed three times and then incubated with secondary antibody for 45 min followed by three washes and final resuspension in PBS. As a negative control, a secondary antibody only sample was used and fluorescence reading from this was used to indicate background fluorescence values. Data was analysed using FlowJo software.

Immunofluorescence and microscopy

Cells were plated onto coverslips or optical plastic bottom dishes coated with human fibronectin (10 ng/mL; Millipore). Following respective treatments, cells were either used for live cell imaging or fixed using 4% paraformaldehyde (PFA/PBS) for 10 mins, washed with PBS and then permeabilised with either methanol at -20°C (for endocytic markers) or 0.2% Triton-X/PBS for 5 mins. Coverslips were then washed with PBS and blocked with 5% BSA/PBS for 30 mins. The primary and secondary antibodies were diluted in 5% BSA/PBS

and incubated for 1 hour each at room temperature with PBS washes between the antibody incubations. Coverslips were mounted onto slides using FluorSave reagent (Calbiochem). Cell images, fixed and live, were acquired on the Nikon A1R confocal microscope (Nikon Instruments UK) at excitation wavelengths 405nm, 488 nm, 543 nm and 633 nm, using a PlanApo VC 60x Oil NA 1.4 objective.

Random migration assay

Cells were seeded onto 12 well plates, starved overnight in Opti-MEM (Gibco) and then stimulated with EGF (10 ng/ml) prior to imaging, which was performed on the Olympus IX71 microscope using an automated x,y,z scanning stage (Ludl). Phase contrast images were acquired using a 10x N-Achroplan NA 0.25 objective and images were taken every 10 mins for 16 hours using a Sensicam (PCO Cook) charge coupled device (CCD) camera and AQM acquisition software (Andor Bioimaging, Belfast, U.K.). Single, non-dividing cells from the time-lapse movies were then tracked using IQ Tracking Software (Andor Bioimaging). The generated position coordinates for each cell per frame were subject to motion analysis using Wolfram Mathematica 6 notebooks to obtain speed measurements.

Fluorescence Recovery After Photobleaching (FRAP) analysis

FRAP experiments were performed on cells stably expressing EGFR-GFP. Live cell images were acquired at 5 sec per frame for 3 frames followed by photobleaching of a circular ROI of 25 pixels in diameter near the cell leading edge using a 488 nm laser at 100% power. Images were acquired for a further 3 minutes at 5 sec per frame. The rate of fluorescence recovery was calculated by measuring the fluorescence intensity of the ROI over time. The fluorescence recovery values were corrected for overall fading across the entire image during the imaging period and were represented as a percentage of the pre-bleached values (the

average values of the first three frames), which represented the 100% fluorescence signal. Values were fitted to a mono-exponential equation from which the T1/2 and the percentage mobile fraction (plateau) values were determined.

Fluorescence Resonance Energy Transfer (FRET) analysis

FRET efficiency was quantified from KS keratinocytes expressing donor and acceptor fluorophores by measuring time domain fluorescence lifetime with a multiphoton microscope system (TE2000, Nikon). Briefly, cells were fixed in 3.6% formaldehyde for 15 minutes, permeabilised with 0.1% Triton and quenched with 1 mg/mL sodium borohydride for 10 minutes at room temperature. Cells were mounted or immunostained for flag detection. Fluorescence lifetime was measured as described previously (Zanet et al., 2012), and histogram data show mean FRET efficiency from denoted numbers of cells per condition in three independent experiments using TRI2 analysis software (Paul Barber, University of Oxford).

Image analysis

All images were analysed using FIJI unless otherwise stated. For quantification of surface levels and total levels of EGFR, images were manually thresholded and intensity values were calculated per cell area and normalised to the control cells in that sample set. Colocalisation analysis was performed on the fixed confocal images using the Coloc2 plugin in FIJI, by either drawing a region of interest (ROI) around the cells to measure total colocalisation within the cell or drawing a 10pix wide line along the leading edge to measure colocalisation at the leading edge. A Python script was created in-house for the analysis of vesicle size, number and EGFR-LAMP1 colocalisation. Vesicles were identified by wavelet filtering the images followed by thresholding and watershed segmentation, using a similar process to that

in (Izeddin et al., 2012). After segmentation, vesicle analysis proceeded using a similar methodology as previously published (Rizk et al., 2014).

Microscale thermophoresis (MST)

Recombinantly expressed kindlin-1 constructs were coupled to an equimolar amount of RED-tris-NTA NT-647 dye (NanoTemper) via its N-terminal 6xHis-Tag in a one-step coupling reaction (Bartoschik et al., 2018). Titrations were performed in phosphate buffered saline (PBS; 137 mM NaCl, 27 mM KCl, 100 mM Na_2HPO_4, 18 mM KH_2PO_4) using a constant 50 nM concentration of RED-tris-NTA coupled kindlin, with increasing concentration of synthetic EGFR peptide (residues 668-711: CMRRRHIVRKRTLRRLLQERELVEPLTPSGEAPNQALLRILKETE); final volume 20 µl. Prepared samples were filled into Monolith NT.115 Capillaries (NanoTemper). Measurements were recorded on a Monolith NT.115 at 25°C, excited under red light, medium MST power and 40% excitation power. The data was analysed using MO Affinity Analysis software and fitted using the K_d fit model.

Statistical analysis

All statistical tests were performed using either T-tests or ANOVA in GraphPad Prism. All data represent at least 3 independent experiments. Statistically significant results were taken as $p<0.05$ and significance values were assigned in specific figures/experiments as shown.

Conflict of interest:

The authors declare no conflicts of interest.

Acknowledgements:

The authors thank Prof David Calderwood, Dr Andy Reynolds, Dr Bob Adelstein and Dr Patrick Caswell for providing plasmids for this study. We also thank the Nikon Imaging Centre@King's for assistance with microscopy and Prof Nick Brown and Dr Silvia Aldaz Casonava for helpful discussions. This work was funded by the Medical Research Council (MR/M018512/1) and the British Skin Foundation. BTG is funded by BBSRC grant (BB/N007336/1) and BTG and AW are funded by HFSP grant (RGP00001/2016).

Author contributions:

MM and RB performed all the experiments, with the exception of MST analysis, which was performed by BTG and AW and FRET/FLIM analysis, which was performed by MP. GKC performed the analysis of Kindlin-2 overexpressing cells. DRM wrote the algorithm and analysed the lysosomal tracking data. WT and KS cells were isolated from patients by JAM. MP, JAM and MM conceived the study and co-wrote the manuscript.

References:

Ashton GH. Kindler syndrome. Clin Exp Dermatol 2004;29(2):116-21.

Baines AJ, Lu HC, Bennett PM. The Protein 4.1 family: hub proteins in animals for organizing membrane proteins. Biochim Biophys Acta 2014;1838(2):605-19.

Bakker J, Spits M, Neefjes J, Berlin I. The EGFR odyssey - from activation to destruction in space and time. J Cell Sci 2017;130(24):4087-96.

Bandyopadhyay A, Rothschild G, Kim S, Calderwood DA, Raghavan S. Functional differences between kindlin-1 and kindlin-2 in keratinocytes. J Cell Sci 2012;125(Pt 9):2172-84.

Banno A, Goult BT, Lee H, Bate N, Critchley DR, Ginsberg MH. Subcellular localization of talin is regulated by inter-domain interactions. J Biol Chem 2012;287(17):13799-812.

Bartoschik T, Galinec S, Kleusch C, Walkiewicz K, Breitsprecher D, Weigert S, et al. Near-native, site-specific and purification-free protein labeling for quantitative protein interaction analysis by MicroScale Thermophoresis. Sci Rep 2018;8(1):4977.

Bialkowska K, Ma YQ, Bledzka K, Sossey-Alaoui K, Izem L, Zhang X, et al. The integrin co-activator Kindlin-3 is expressed and functional in a non-hematopoietic cell, the endothelial cell. J Biol Chem 2010;285(24):18640-9.

Bouaouina M, Goult BT, Huet-Calderwood C, Bate N, Brahme NN, Barsukov IL, et al. A conserved lipid-binding loop in the kindlin FERM F1 domain is required for kindlin-mediated alphaIIbbeta3 integrin coactivation. J Biol Chem 2012;287(10):6979-90.

Brahme NN, Harburger DS, Kemp-O'Brien K, Stewart R, Raghavan S, Parsons M, et al. Kindlin binds migfilin tandem LIM domains and regulates migfilin focal adhesion localization and recruitment dynamics. J Biol Chem 2013;288(49):35604-16.

Campbell P, Morton PE, Takeichi T, Salam A, Roberts N, Proudfoot LE, et al. Epithelial inflammation resulting from an inherited loss-of-function mutation in EGFR. J Invest Dermatol 2014;134(10):2570-8.

Caswell PT, Spence HJ, Parsons M, White DP, Clark K, Cheng KW, et al. Rab25 associates with alpha5beta1 integrin to promote invasive migration in 3D microenvironments. Dev Cell 2007;13(4):496-510.

Duan L, Miura Y, Dimri M, Majumder B, Dodge IL, Reddi AL, et al. Cbl-mediated ubiquitinylation is required for lysosomal sorting of epidermal growth factor receptor but is dispensable for endocytosis. J Biol Chem 2003;278(31):28950-60.

Goult BT, Bouaouina M, Harburger DS, Bate N, Patel B, Anthis NJ, et al. The structure of the N-terminus of kindlin-1: a domain important for alphaiibbeta3 integrin activation. J Mol Biol 2009;394(5):944-56.

Guo B, Gao J, Zhan J, Zhang H. Kindlin-2 interacts with and stabilizes EGFR and is required for EGF-induced breast cancer cell migration. Cancer Lett 2015;361(2):271-81.

Has C, Castiglia D, del Rio M, Diez MG, Piccinni E, Kiritsi D, et al. Kindler syndrome: extension of FERMT1 mutational spectrum and natural history. Hum Mutat 2011;32(11):1204-12.

Has C, Ludwig RJ, Herz C, Kern JS, Ussar S, Ochsendorf FR, et al. C-terminally truncated kindlin-1 leads to abnormal adhesion and migration of keratinocytes. Br J Dermatol 2008;159(5):1192-6.

Herz C, Aumailley M, Schulte C, Schlotzer-Schrehardt U, Bruckner-Tuderman L, Has C. Kindlin-1 is a phosphoprotein involved in regulation of polarity, proliferation, and motility of epidermal keratinocytes. J Biol Chem 2006;281(47):36082-90.

Huet-Calderwood C, Brahme NN, Kumar N, Stiegler AL, Raghavan S, Boggon TJ, et al. Differences in binding to the ILK complex determines kindlin isoform adhesion localization and integrin activation. J Cell Sci 2014;127(Pt 19):4308-21.

Izeddin I, El Beheiry M, Andilla J, Ciepielewski D, Darzacq X, Dahan M. PSF shaping using adaptive optics for three-dimensional single-molecule super-resolution imaging and tracking. Opt Express 2012;20(5):4957-67.

Jobard F, Bouadjar B, Caux F, Hadj-Rabia S, Has C, Matsuda F, et al. Identification of mutations in a new gene encoding a FERM family protein with a pleckstrin homology domain in Kindler syndrome. Hum Mol Genet 2003;12(8):925-35.

Kim JH, Wang A, Conti MA, Adelstein RS. Nonmuscle myosin II is required for internalization of the epidermal growth factor receptor and modulation of downstream signaling. J Biol Chem 2012;287(33):27345-58.

Lai-Cheong JE, Liu L, Sethuraman G, Kumar R, Sharma VK, Reddy SR, et al. Five new homozygous mutations in the KIND1 gene in Kindler syndrome. J Invest Dermatol 2007;127(9):2268-70.

Lai-Cheong JE, Tanaka A, Hawche G, Emanuel P, Maari C, Taskesen M, et al. Kindler syndrome: a focal adhesion genodermatosis. Br J Dermatol 2009;160(2):233-42.

Lai-Cheong JE, Ussar S, Arita K, Hart IR, McGrath JA. Colocalization of kindlin-1, kindlin-2, and migfilin at keratinocyte focal adhesion and relevance to the pathophysiology of Kindler syndrome. J Invest Dermatol 2008;128(9):2156-65.

Larjava H, Plow EF, Wu C. Kindlins: essential regulators of integrin signalling and cell-matrix adhesion. EMBO Rep 2008.

Liu Z, Lu D, Wang X, Wan J, Liu C, Zhang H. Kindlin-2 phosphorylation by Src at Y193 enhances Src activity and is involved in Migfilin recruitment to the focal adhesions. FEBS Lett 2015;589(15):2001-10.

Maiuri P, Terriac E, Paul-Gilloteaux P, Vignaud T, McNally K, Onuffer J, et al. The first World Cell Race. Curr Biol 2012;22(17):R673-5.

Meves A, Stremmel C, Gottschalk K, Fassler R. The Kindlin protein family: new members to the club of focal adhesion proteins. Trends Cell Biol 2009;19(10):504-13.

Qu H, Tu Y, Guan JL, Xiao G, Wu C. Kindlin-2 tyrosine phosphorylation and interaction with Src serve as a regulatable switch in the integrin outside-in signaling circuit. J Biol Chem 2014;289(45):31001-13.

Reynolds AR, Tischer C, Verveer PJ, Rocks O, Bastiaens PI. EGFR activation coupled to inhibition of tyrosine phosphatases causes lateral signal propagation. Nat Cell Biol 2003;5(5):447-53.

Rizk A, Paul G, Incardona P, Bugarski M, Mansouri M, Niemann A, et al. Segmentation and quantification of subcellular structures in fluorescence microscopy images using Squassh. Nat Protoc 2014;9(3):586-96.

Rognoni E, Ruppert R, Fassler R. The kindlin family: functions, signaling properties and implications for human disease. J Cell Sci 2016;129(1):17-27.

Siegel DH, Ashton GH, Penagos HG, Lee JV, Feiler HS, Wilhelmsen KC, et al. Loss of kindlin-1, a human homolog of the Caenorhabditis elegans actin-extracellular-matrix linker protein UNC-112, causes Kindler syndrome. Am J Hum Genet 2003;73(1):174-87.

Singh B, Coffey RJ. Trafficking of epidermal growth factor receptor ligands in polarized epithelial cells. Annu Rev Physiol 2014;76:275-300.

Techanukul T, Sethuraman G, Zlotogorski A, Horev L, Macarov M, Trainer A, et al. Novel and recurrent FERMT1 gene mutations in Kindler syndrome. Acta Derm Venereol 2011;91(3):267-70.

Wiebe CB, Petricca G, Hakkinen L, Jiang G, Wu C, Larjava HS. Kindler syndrome and periodontal disease: review of the literature and a 12-year follow-up case. J Periodontol 2008;79(5):961-6.

Worth DC, Hodivala-Dilke K, Robinson SD, King SJ, Morton PE, Gertler FB, et al. Alpha v beta3 integrin spatially regulates VASP and RIAM to control adhesion dynamics and migration. J Cell Biol 2010;189(2):369-83.

Zanet J, Jayo A, Plaza S, Millard T, Parsons M, Stramer B. Fascin promotes filopodia formation independent of its role in actin bundling. J Cell Biol 2012;197(4):477-86.

Zhang G, Gu Y, Begum R, Chen H, Gao X, McGrath JA, et al. Kindlin-1 Regulates Keratinocyte Electrotaxis. J Invest Dermatol 2016;136(11):2229-39.

Figure Legends:

Figure 1: EGFR levels are reduced in keratinocytes lacking kindlin-1

(a,b) Levels of EGFR protein (a) and (mRNA (b) in wild-type (WT) and Kindler Syndrome (KS) keratinocytes. (c) Western blot of EGFR levels in WT, KS cells, KS re-expressing mCherry-kindlin-1. (d) Quantification of EGFR surface levels in WT and KS cells by FACS. (e) Immunostaining of WT and KS skin for EGFR (green) and DAPI (blue). White line indicates dermal-epidermal junction. (f,g) Analysis of EGFR (f) and ERK1/2 phosphorylation (g) in WT and KS cells following 10 mins EGF stimulation. GAPDH was used as a loading control for western blots. Data are means ± SEM; **P<0.01 by T-test. Scale bar, 20μm.

Figure 2: EGFR localises to lysosomal compartments in KS cells.

(a) Immunostaining of EGFR (green) and F-actin (magenta) and (b) quantification of EGFR surface and (c) total levels from images in WT and KS cells following EGF stimulation. (d) Immunostaining and quantification of EGFR (green) localisation with EEA1, (e) LAMP1 or (f) Rab11a vesicles (all shown in magenta) following EGF stimulation (10ng/ml). Graphs beneath images show Pearson's correlation coefficient analysis of EGFR and specified compartments. N=30 cells for each. (g) Still images from movies of WT and KS cells expressing EGFR-GFP labelled with lysotracker deep red (magenta) following EGF stimulation. (h) Quantification of number of EGFR positive vesicles and (i) EGFR/lysotracker colocalisation from WT and KS movies. N=25 cells over 3 independent experiments. Data are all means ± SEM; ***P<0.001, **P<0.01, ***P<0.001 using two-way ANOVA (b and c) and T-test (D-F). Scale bars are 10μm throughout.

Figure 3: EGFR is degraded in the lysosome in KS cells through increased Cbl interactions.

(a-c) Treatment of WT and KS cells with proteasome inhibitor (MG132; 10μM, 24hr; a) or lysosome inhibitors leupeptin (LP; 100nM, 24hr; b) or Concanamycin A (ConA; 100nM, 24hr; c) and analysis of EGFR levels by western blotting. (d) Quantification of western blots in A-C from 4 independent experiments. (e) Immunoprecipitation of EGFR from WT and KS cells following DMSO (-) or ConA treatment (100nM, 24hr; +) and immunoblotting for c-Cbl. Blots beneath show c-Cbl levels in whole cell lysates.

Figure 4: EGFR directly interacts with kindlin-1 via the F1loop region.

(a) Diagram of GST and His tagged kindlin protein domains used. (b) GST pulldown of kindlin-1 domains and immunoblotting for EGFR in WT keratinocytes. Quantification of GST-K1 domains and EGFR interaction shown in graph. (c) His kinesin light chain (-ve control) or kindlin-1 F1 Loop incubated with purified GST-EGFR cytoplasmic domain. (d) *In vitro* binding of GST-EGFR cytoplasmic tail and His-kindlin F1 loop (His1) using GST pulldown. (e) MST analysis of full length (black) or F0F1 (green) kindlin-1 and EGFR cytoplasmic tail interaction. R7-R9 of Talin (blue) was used as a control. All data are means ± SEM from 3 independent experiments; ** $P< 0.01$, using one-way ANOVA.

Figure 5: EGFR-kindlin-1 binding in human keratinocytes is EGF regulated.

(a) SIM imaging of EGFR-GFP (green) and mCherry-kindlin-1 (magenta) following EGF stimulation. Inset boxes shown below each time point. (b) Immunoprecipitation of EGFR from KS cells re-expressing mCherry-kindlin-1 under starved conditions or after EGF stimulation (10ng/ml). Graph on right shows quantification of 5 independent experiments. (c) Example lifetime images of KS cells expressing kindlin-GFP and mCherry-kindlin-1 following EGF stimulation. Graph on right shows quantification of 25 cells per condition over 3 experiments. (d) Example images of KS cells re-expressing mCherry-kindlin-1

(magenta) under growth conditions with DMSO or AG1478 treatment, fixed and stained for EGFR (green). Inset boxes shown below. Graph on right show quantification of colocalisation from 30 cells. (e) Immunoprecipitation of GFP or GFP-kindlin-1 under same conditions as in (d), probed for phosphotyrosine (pY) and GFP *P<0.05, **P<0.01, using two-way ANOVA. Scale bars are 1μm in (a) and 10μm in (c) and (d).

Figure 1

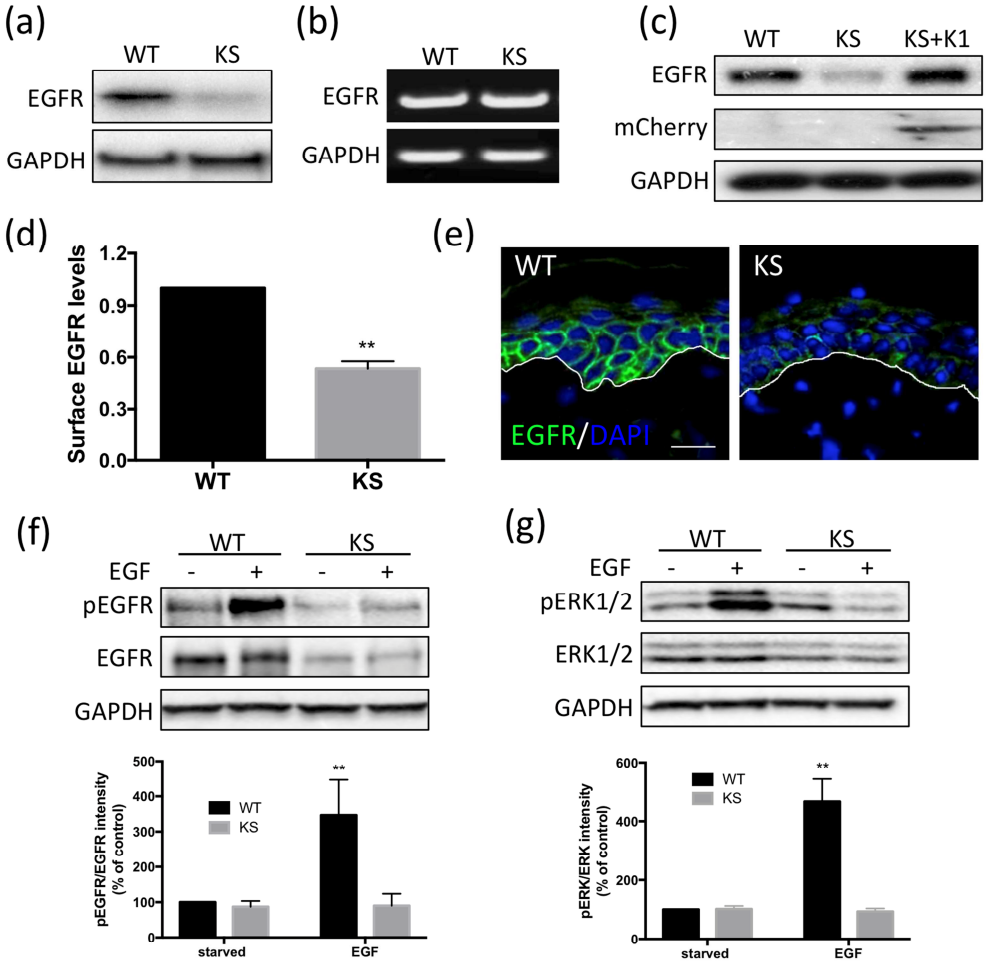
(a)
WT
KS
EGFR
GAPDH
(b)
WT
KS
EGFR
GAPDH
(c)
WT
KS
KS+K1
EGFR
mCherry
GAPDH
(d)
Surface EGFR levels
1.2
0.9
0.6
0.3
0.0
**
WT
KS
(e)
WT
KS
EGFR/DAPI
(f)
WT
KS
EGF
- + - +
pEGFR
EGFR
GAPDH
pEGFR/EGFR intensity (% of control)
500
400
300
200
100
0
WT
KS
**
starved
EGF
(g)
WT
KS
EGF
- + - +
pERK1/2
ERK1/2
GAPDH
pERK/ERK intensity (% of control)
600
400
200
0
WT
KS
**
starved
EGF

Figure 2

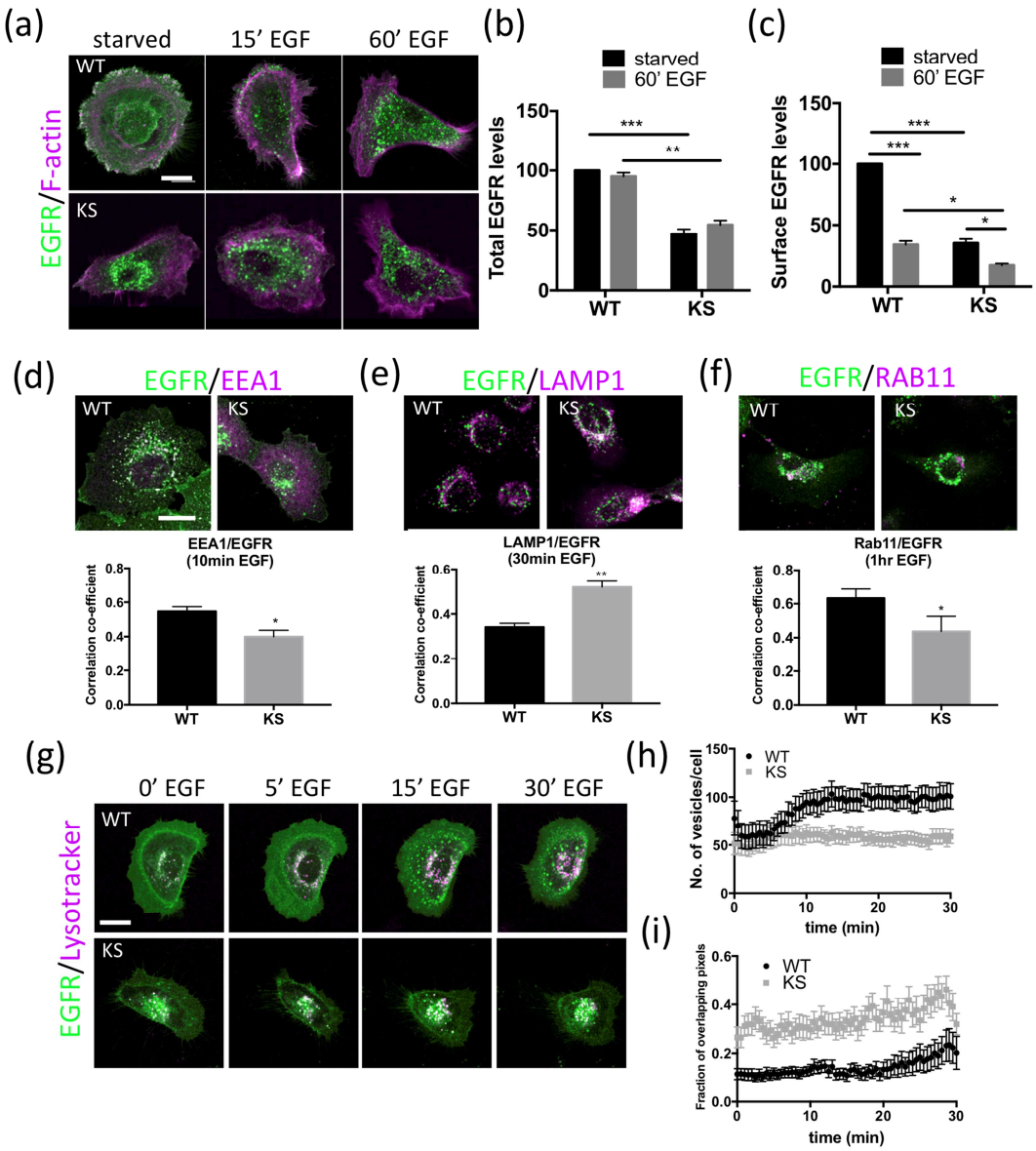
(a)
starved
15' EGF
60' EGF
WT
KS
EGFR/F-actin
(b)
starved
60' EGF
Total EGFR levels
150
100
50
0
***
**
WT
KS
(c)
starved
60' EGF
Surface EGFR levels
150
100
50
0
***
***
*
*
WT
KS
(d)
EGFR/EEA1
WT
KS
EEA1/EGFR
(10min EGF)
Correlation co-efficient
0.8
0.6
0.4
0.2
0.0
*
WT
KS
(e)
EGFR/LAMP1
WT
KS
LAMP1/EGFR
(30min EGF)
Correlation co-efficient
0.6
0.4
0.2
0.0
**
WT
KS
(f)
EGFR/RAB11
WT
KS
Rab11/EGFR
(1hr EGF)
Correlation co-efficient
0.8
0.6
0.4
0.2
0.0
*
WT
KS
(g)
0' EGF
5' EGF
15' EGF
30' EGF
WT
KS
EGFR/Lysotracker
(h)
No. of vesicles/cell
150
100
50
0
WT
KS
0
10
20
30
time (min)
(i)
Fraction of overlapping pixels
0.6
0.4
0.2
0.0
WT
KS
0
10
20
30
time (min)

Figure 3

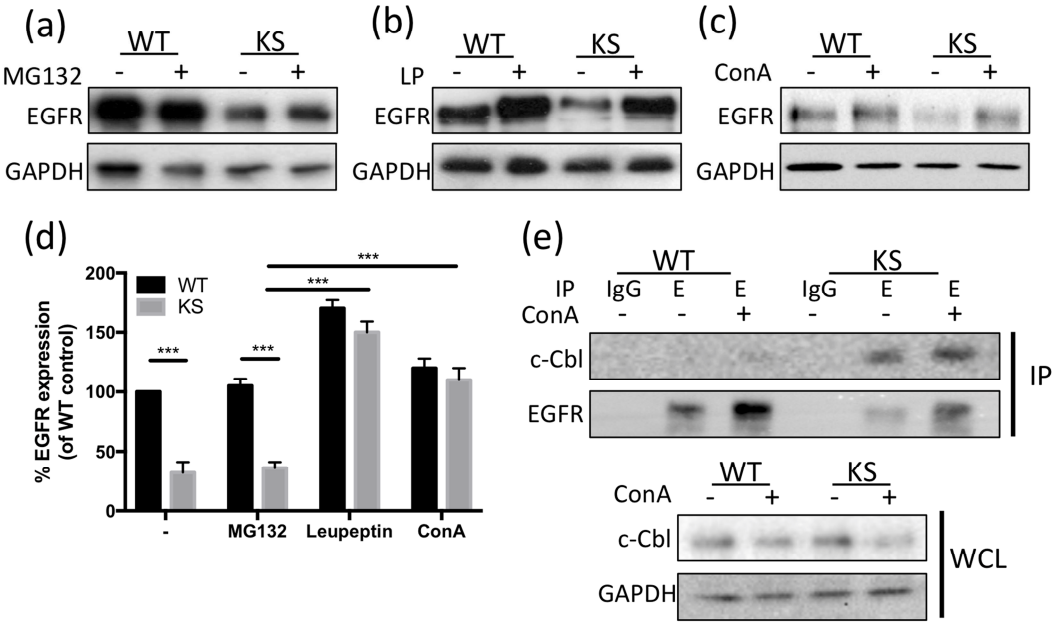
(a)
WT
KS
MG132
- + - +
EGFR
GAPDH
(b)
WT
KS
LP
- + - +
EGFR
GAPDH
(c)
WT
KS
ConA
- + - +
EGFR
GAPDH
(d)
% EGFR expression (of WT control)
200
150
100
50
0
WT
KS
***
***
***
***
-
MG132
Leupeptin
ConA
(e)
WT
KS
IP
IgG
E
E
IgG
E
E
ConA
- - + - - +
c-Cbl
EGFR
IP
WT
KS
ConA
- + - +
c-Cbl
GAPDH
WCL

Figure 4

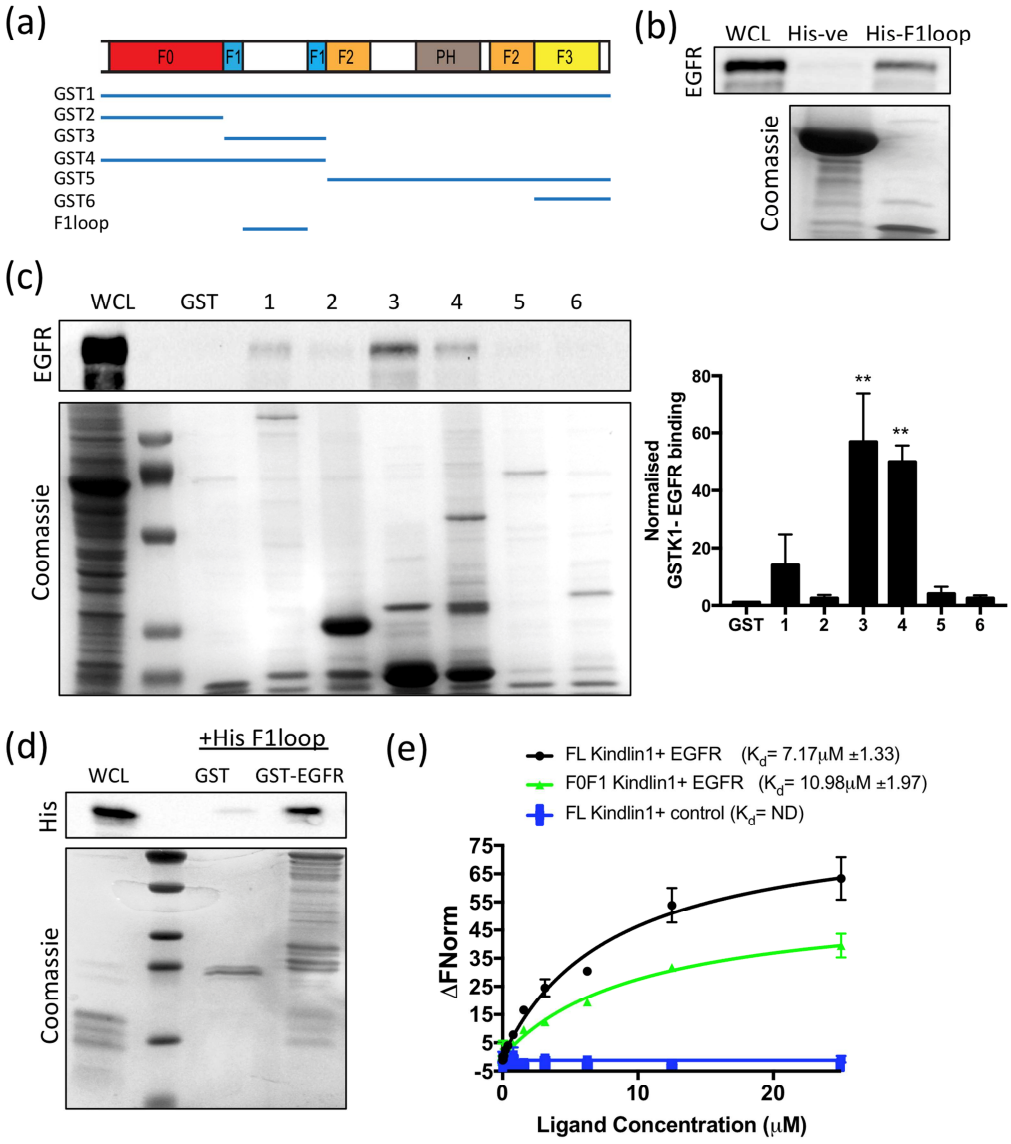
(a)
F0
F1
F1
F2
PH
F2
F3
GST1
GST2
GST3
GST4
GST5
GST6
F1loop
(b)
WCL
His-ve
His-F1loop
EGFR
Coomassie
(c)
WCL
GST
1
2
3
4
5
6
EGFR
Coomassie
Normalised GSTK1- EGFR binding
80
60
40
20
0
**
**
GST
1
2
3
4
5
6
(d)
+His F1loop
WCL
GST
GST-EGFR
His
Coomassie
(e)
FL Kindlin1+ EGFR (Kd= 7.17μM ±1.33)
F0F1 Kindlin1+ EGFR (Kd= 10.98μM ±1.97)
FL Kindlin1+ control (Kd= ND)
ΔFNorm
75
65
55
45
35
25
15
5
-5
0
10
20
Ligand Concentration (μM)

Figure 5

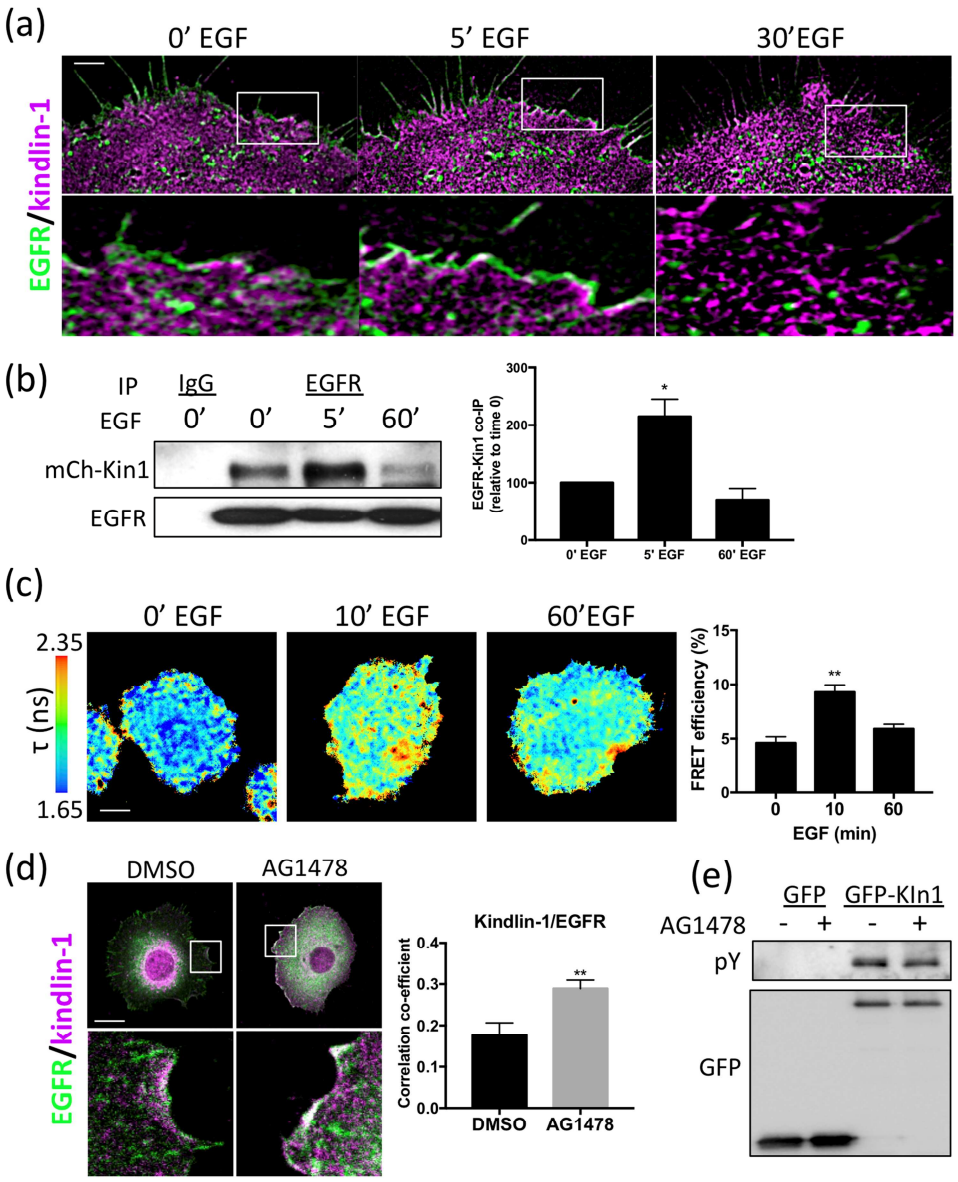
(a)
0' EGF
5' EGF
30'EGF
EGFR/kindlin-1
(b)
IP
IgG
EGFR
EGF
0'
0'
5'
60'
mCh-Kin1
EGFR
EGFR-Kin1 co-IP (relative to time 0)
300
200
100
0
*
0' EGF
5' EGF
60' EGF
(c)
0' EGF
10' EGF
60'EGF
2.35
τ (ns)
1.65
FRET efficiency (%)
15
10
5
0
**
0
10
60
EGF (min)
(d)
DMSO
AG1478
EGFR/kindlin-1
Kindlin-1/EGFR
Correlation co-efficient
0.4
0.3
0.2
0.1
0.0
**
DMSO
AG1478
(e)
GFP
GFP-KIn1
AG1478
-
+
-
+
pY
GFP